A finite-difference model of temperatures and heat flow within a tree stem

Brian E. Potter and Jeffrey A. Andresen

Abstract: The authors present a finite-difference numerical model of heat flow within a horizontal section of a tree stem. Processes included in the model are solar radiative heating, infrared emission and absorption, convective heat exchange between tree surface and the atmosphere, and conduction inside the tree. Input variables include wood density, wood thermal conductivity, wood specific heat, wind speed, air temperature, and insolation. The model produces time series of temperature for grid points inside the tree stem. Based on comparison with observations from two case studies, the model appears capable of reproducing relative timing and amplitude of temperature patterns at the cardinal aspects. Sensitivity tests show that insolation and convection parameters, as well as the physical properties of the tree, can all have a strong influence on model results.

Résumé : Les auteurs présentent un modèle numérique basé sur la méthode des différences finies du flux de chaleur au travers d'une section horizontale de la tige d'un arbre. Les processus inclus dans le modèle sont le réchauffement dû au rayonnement solaire, l'émission et l'absorption dans l'infrarouge, l'échange d'énergie par convection entre la surface de l'arbre et l'atmosphère et la conduction à l'intérieur de l'arbre. Les variables d'entrée sont la densité du bois, la conductivité thermique du bois, la chaleur spécifique du bois, la vitesse du vent, la température de l'air et l'ensoleillement. Le modèle génère une série chronologique de températures pour une grille de points à l'intérieur de la tige de l'arbre. Sur la base d'une comparaison avec les observations de deux études de cas, le modèle semble capable de reproduire la séquence relative et l'amplitude des patrons de température aux points cardinaux. Des tests de sensibilité montrent que les paramètres d'insolation et de convection, de même que les propriétés physiques de l'arbre, peuvent tous fortement influencer les résultats du modèle.

[Traduit par la Rédaction]

Introduction

Temperatures and energy fluxes within and on a tree stem are of interest to several areas of research. Fire ecologists and tree physiologists need to know how fire affects cambium temperatures and the role of bark as an insulator (e.g., Hare 1965; Gill and Ashton 1968; Vines 1968; Hengst and Dawson 1994). Horticulturists are concerned with preventing thaw–freeze damage in fruit trees (Eggert 1944; Derby and Gates 1966). For some insect species, tree surface and interior temperatures influence development and mortality (Shepherd 1966; Greaves 1965; T. Poland, personal communication[2]). Similarly, the germination and spread of fungi are temperature dependent (Hayes and Manap 1975; Dickenson and Wheeler 1981).

Most studies of temperatures within and on trees have used thermometers or thermocouples inserted in the tree or attached to the bark. Both options involve physical alteration of the tree studied, and the sensor can alter the temperature by conducting heat into or out of the tree (Derby and Gates 1966). Attempts by Derby and Gates (1966) and Herrington (1969) to develop computer models of the temperature and heat flow in a tree showed the potential of such models as an economical and plausible alternative to installing and monitoring instruments in the field.

For whatever reason, work on modeling tree heat and temperature has not been carried forward in the open literature. With the computers available today, it is possible to create and run faster models with higher resolution and greater detail than what these earlier authors were able to use. Furthermore, technological advances have allowed significant advances in the numerical methods one can use in a computer model. In this paper, we present a finite-difference numerical model of heat flow within a horizontal slice of a tree stem and between the stem and its environment. We describe the numerical techniques for this model and present the results of two case studies comparing the model with observational data. We also show the results of sensitivity tests on five of the more critical and potentially uncertain parameters in the model.

Received 28 March 2001. Accepted 3 December 2001. Published on the NRC Research Press Web site at http://cjfr.nrc.ca on 12 March 2002.

B.E. Potter.[1] USDA Forest Service, North Central Research Station, 1407 S. Harrison Rd, Suite 220, East Lansing, MI 48823, U.S.A.
J.A. Andresen. Department of Geography, Michigan State University, East Lansing, MI 48824, U.S.A.

[1]Corresponding author (e-mail: bpotter@fs.fed.us).
[2]Dr. Therese Poland, USDA Forest Service, 1407 S. Harrison Road, East Lansing, MI 48823, U.S.A.

 DOI: 10.1139/X01-226

Theory

We consider two-dimensional heat flow within a circular, horizontal section of a tree (Fig. 1), for which polar coordinates are appropriate. The processes we include in the model are conduction within the tree, convective heat exchange with surrounding air, solar radiative heating, and long wave (infrared) radiative exchange with the surrounding environment. Conduction is the only process that occurs inside the tree, all other processes apply only at the tree's outer surface.

The basic heat equation for conduction is

$$[1] \qquad \rho c \frac{\partial T}{\partial t} = \nabla \cdot (k \nabla T)$$

where ρ is density ($kg \cdot m^{-3}$), c is specific heat ($J \cdot kg^{-1} \cdot K^{-1}$), T is temperature (K), t is time (s), and k is thermal conductivity ($W \cdot m^{-1} \cdot K^{-1}$). In polar coordinates, eq. 1 becomes

$$[2] \qquad \rho c \frac{\partial T}{\partial t} = \frac{1}{r} \frac{\partial}{\partial r} \left(kr \frac{\partial T}{\partial r} \right) + \frac{1}{r} \frac{\partial}{\partial \phi} \left(\frac{k}{r} \frac{\partial T}{\partial \phi} \right)$$

where r is distance from the center of the tree and ϕ is azimuth angle (measured clockwise with south being $\phi = 0$). In this model, we assume that conductivity is independent of azimuth, i.e., $\partial k / \partial \phi = 0$.

Convective heat loss can be either free or forced. Free convection occurs when the tree surface temperature differs from that of the ambient atmosphere; the tree surface thus warms or cools the air adjacent to it by contact and losses or gains heat in the process. This occurs whether or not there is wind. Forced convection is the loss or gain of energy by the tree surface resulting from a colder or warmer wind blowing across it. Convective heat loss, H, is expressed as

$$[3] \qquad H = h(T_{sfc} - T_{air})$$

where h ($W \cdot m^{-2} \cdot K^{-1}$) is the convective heat transfer coefficient. The full convective heat transfer coefficient, h, is the sum of h_{free} and h_{forced}.

For free convection, h_{free} is parameterized as

$$[4] \qquad h_{free} = 18.293 \left(\frac{|T_{sfc} - T_{air}|}{L T_{air}^3} \right)^{0.25} \left(\frac{T_{air} + 97.77}{\sqrt{179.02 + T_{air}}} \right)$$

Here, L is the vertical length (assumed to be 1 m in this model) of the surface element being considered. The Appendix contains details of the derivation of eq. 4.

The heat transfer coefficient for forced convection follows the formula in Kreith and Bohn (1986) for heat transfer from a cylinder, with conversion to SI units. The result is

$$[5] \qquad h_{forced} = 3.458(T_{air} + T_{sfc} - 0.74)^{0.49} \left(\frac{u}{R T_{air}} \right)^{0.5} \times \left[1 - \left(\frac{\theta}{90} \right)^3 \right]$$

Fig. 1. Model geometry. Each element has radial width Δr and angular width Δf. Angles are measured clockwise from south.

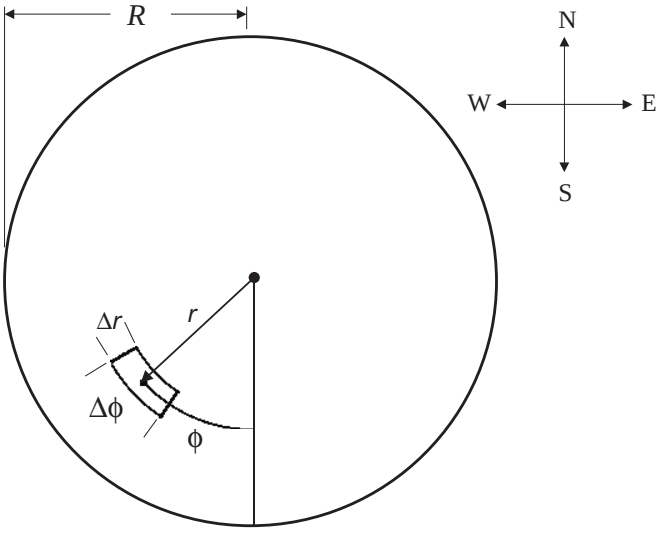

Here u is the wind speed ($m \cdot s^{-1}$) and R is the radius of the tree (m). The angle θ is the lesser of 90° or the difference between wind direction and the aspect of the surface point.

The convective formulation presented here assumes certain types of atmospheric conditions. Specifically, eq. 4 is strictly valid only if the Grashof number, described in the Appendix, is less than 10^9. For situations with large air–surface temperature differences, it should be replaced by a different parameterization. Similarly, eq. 5 applies for Reynolds numbers (Re) between 10^3 and 10^5. At higher Re (i.e., faster winds or larger diameter trees), both the temperature-dependent portion and the wind-angle portion of eq. 5 would change as a result of more turbulent flow and eddies on the lee side of the tree. Even as it is written, eq. 5 is likely to underestimate h_{forced} on the tree's lee side for moderately high wind speeds.

The incident solar energy at a point on the tree surface depends on the aspect angle of the point, the time of day, the day of the year, and the latitude and longitude of the tree. Furthermore, sunlight reaching a point can be either direct or diffuse. To determine incident solar radiation at a surface point, we used standard astronomical equations to determine the solar zenith and azimuth angles (Lowry and Lowry 1989) and subsequently the angle of incidence for a given point on the tree. Direct solar radiation incident at the point is then

$$[6] \qquad S_{dir} = S_0(\tau)^{\sec Z} \cos(i)$$

where S_0 is the solar constant, 1368 $W \cdot m^{-2}$, τ is atmospheric transmissivity (unitless), Z is the solar zenith angle, and i is the angle of incidence (i.e., the angle between the direction of the sunlight and the local normal to the tree's surface) at the point in question. When i is greater than 90°, the sun is behind the tree and S_{dir} is zero at that point.

We assume diffuse solar radiation is independent of aspect angle and compute the magnitude according to Lowry and Lowry (1989):

$$[7] \qquad S_{dif} = \frac{S_0 \cos Z}{3}(1 + \cos Z)[\eta - (\tau)^{\sec Z}]$$

where η is the atmospheric absorption parameter (unitless). For midlatitude, low elevation (0 to 1 km above sea level) situations, Lowry and Lowry (1989) state that typical values for τ range from 0.76 to 0.81, and that values for η range from 0.80 to 0.84.

Total solar radiation incident at a specific surface point is the sum of S_{dir} and S_{dif}, while the amount of solar radiation absorbed also depends on the albedo of the surface, α. Equations 6 and 7 are for cloudless skies and will yield too much direct and too little diffuse radiation under cloudy conditions.

The tree surface emits long wave radiation, and at the same time it receives long wave radiation from the surrounding air and other vegetation. We assume that the tree emits as a black body:

$$[8] \qquad IR_{out} = \sigma T_{sfc}^4$$

and that the environment radiates as a black body at the temperature of the surrounding air:

$$[9] \qquad IR_{in} = \sigma T_{air}^4$$

where σ is the Stefan–Boltzmann constant, 5.67×10^{-8} W·m^{-2}·K^{-4}. In reality, the incoming radiation comes from plants, rocks, soil, and air at various levels and therefore various temperatures. Trying to include an accurate representation of so many features in any realistic way is practically impossible, so we settled on using the ambient air temperature as a reasonable approximation.

The complete thermodynamic equation used in the model is then

$$[10] \qquad \rho c \frac{\partial T}{\partial t} = \nabla \cdot (k \nabla T) - \frac{1}{\Delta r}[H + (1 - \alpha)(S_{dir} + S_{dif}) + (IR_{in} - IR_{out})]$$

The term $(1/\Delta r)$ appears because the quantities in brackets are all surface energy fluxes, while the conduction terms apply to the model element volume.

In this model, we do not consider heat transported into or out of an element by sap flow. The two-dimensionality of the model is the main reason for this, since sap flow is perpendicular to the plane of the section considered here. In some species and seasons, sap flow may transport significant amounts of heat and the heat flux could be comparable to some of the other heat transfer processes we do include. This model would not be suitable for such situations without added assumptions or conversion to three dimensions.

A second type of heat transfer neglected in this model involves water on the outer tree surface. Condensation and evaporation will act to warm and cool the surface, respectively. Precipitation would cool or warm the tree surface, depending on the relative temperatures of the precipitation and the tree. Because of the complexity of modeling condensation and the difficulty in determining precipitation temperatures, we exclude them here.

The processes outlined above include several coefficients that depend on the exact situation being modeled. These include ρ, c, k, u, τ, η, and T_{air}. The first three depend on the type of tree being considered and on the moisture content of that tree. The wind speed, u, atmospheric absorption properties, τ and η, and air temperature, T_{air}, can be either prescribed or come from observations.

Numerical methods

The model divides the horizontal disk into N_r radial elements of width $\Delta r = R/N_r$ and N_ϕ angular elements of angular width $\Delta\phi = 2\pi/N_\phi$, as shown in Fig. 1. Temperatures, densities, specific heats, and thermal conductivities at the model grid points represent the mean value within their respective elements.

We compute spatial derivatives in the model using a second-order centered differencing scheme, as described in Haltiner and Williams (1980). Temporal derivatives use a centered leapfrog scheme with an Asselin filter for smoothing and elimination of computational modes (Haltiner and Williams 1980). We used a smoothing coefficient of $\gamma = 0.2$.

At the outer boundary, we computed $\partial T/\partial r$ using a second-order difference with the environmental temperature, T_{air}, as the outward temperature. The second derivative, $\partial^2 T/\partial r^2$, is computed using first-order differences with T_{air} as the outermost temperature.

Case studies

We evaluated the model's performance by comparing its output with observational data provided in Derby and Gates (1966). They present two separate data sets that were amenable to this: one set of temperatures measured in a vertical pine log (*Pinus contorta* Dougl. ex Loud.) and one set of temperatures measured in a living aspen tree (*Populus* sp.). Information on the trees and their locations could be found in Derby and Gates (1966), and we were able to obtain hourly air and tree temperature data from their figures.

The pine log data came from a log 0.18 m in diameter and 2.4 m tall. (Details of the instrument installation are in the original paper.) For albedo, we assumed a value of 0.3. This is a rough estimate based on the albedo of 0.45 that Derby and Gates provide for aspen, and the albedo of 0.27 for white oak (*Quercus alba* L.) bark given in Andresen et al. (2001). The temperatures Derby and Gates present were measured on October 28 and 29, 1965, in Boulder, Colorado (latitude 40.0°N, elevation 1630 m.) Though they measured temperatures at 13 points in the log, we used only the data taken at 0.048 m from the log center in the four cardinal compass directions for our test. We used hourly wind observations from the National Weather Service for Denver's Stapleton Airport.

For solar radiation, we used cloud observations from Stapleton Airport in conjunction with the previously described analytical equations of insolation. We specified $\tau = 0.78$ and $\eta = 0.80$ for these tests, based on Lowry and Lowry (1989) and the elevation of the observation site. Over the day on October 28, the fraction of the sky covered by cloud ranged from 0.5 to 1.0, and the fraction described as opaque was from 0 to 0.8. As a crude approximation, we specified that direct radiation in the model would be full strength for the fraction of sky uncovered by cloud, 80% of full for the

Table 1. Parameter values used for model performance tests.

Parameter (units)	Pine test	Aspen test
Calendar day	301	92
Latitude (°N)	40.0	39.8
Tree radius (m)	0.09	0.075
Density ($kg \cdot m^{-3}$)	686	714
Specific heat ($J \cdot kg^{-1} \cdot K^{-1}$)	2470	2670
Conductivity ($W \cdot m^{-1} \cdot K^{-1}$)	0.46	0.57
Albedo	0.3	0.45

fraction that was cloudy but not opaque, and 10% of full for the fraction that was opaque cloud:

$$[11] \quad S = (1 - F_t)D + 0.8(F_t - F_q)D + 0.1F_qD$$

where S is the direct insolation incident on a normal (angle of incidence from the normal equal to zero) surface, F_t is the fraction of the sky with cloud, F_q is the fraction covered by opaque cloud, and D is the analytical maximum insolation on the tree for that time and aspect. This is extremely crude, but we feel it is at least more realistic than using full, analytical insolation. Diffuse radiation was not modified from the Lowry and Lowry (1989) based values. This may underestimate diffuse radiation under clouds, but given the crude nature of eq. 11, we chose not to alter the diffuse equation, effectively placing all assumptions in eq. 11.

The live aspen temperature measurements took place on April 2 and 3, 1965, near Blackhawk, Colorado (latitude 39.8°N, elevation 2820 m). The tree was 0.15 m in diameter, situated on the south side of a stand of aspen, and the description of the weather Derby and Gates provide is "clear and calm in the early mornings; cool, cloudy and windy in the afternoons". Following their procedure, we specified a constant 2.7 $m \cdot s^{-1}$ (6 mi/h) wind from the west. We used full analytical insolation and did not adjust for clouds, primarily because cloud observations are not available near the site and in mountainous regions such as this, assuming the same cloud cover as the nearest weather station (Denver, roughly 50 km away and 1200 m lower) would be difficult to justify. In these tests, we specified $\tau = 0.85$ and $\eta = 0.88$, based on Lowry and Lowry (1989) and the elevation of the observation site. Following Derby and Gates (1966), we used an albedo of 0.45 for this tree.

Values for density, conductivity, and specific heat were absent from Derby and Gates. Since these are essential for the model, we relied on the information in TenWolde et al. (1988) and Forest Products Laboratory (1987) to determine physically reasonable values for the needed parameters. Because ρ, c, and k are all proportional to moisture content, we determined limiting reasonable values for moisture content and derived the other variables from these. The results that follow are for the parameter values shown in Table 1, and model sensitivity to these parameters is discussed in the next section. In both cases, we used $N_r = 10$ and $N_\phi = 20$.

For each of the comparisons, we used mean error and root mean square error as measures of the model's performance. We calculated these measures on each of the four cardinal aspects and for all four aspects combined.

Figure 2 shows the model results for the vertical pine log, along with the observed values taken from Derby and Gates (1966). The model errors are summarized in Table 2. For the north aspect, model temperatures were too high during the day and too low at night. The west aspect was similar but the model became too cool shortly after 12:00 local standard time (LST). On the south and east aspects, temperatures were too cool except at 12:00 and 13:00 LST on the east. All four aspects reach their peak temperature around 15:00 LST, which agrees with the observed conditions. Furthermore, the broad plateau for the east and the sharp peak on the west that appear in the observations are reproduced by the model.

Figure 3 and Table 2 provide the aspen results. The north, south, and west aspects showed temperatures consistently warmer than those observed, but which appeared to be dropping below the observed temperatures at the end of the test run. The east aspect started out warmer than observed, became cooler for a couple of hours, then became warmer than the observed temperatures again. This test only included 1 h when the sun was not up, so the model's performance at night cannot be assessed.

The energy fluxes for the north and south surface points in the aspen simulations are shown in Fig. 4. On the north, diffuse solar radiation was fairly steady around 30 $W \cdot m^{-2}$ all day. Conduction of heat from within the tree increased from 10:00 LST onward and peaked at 18:00 LST. Convection, on the other hand, cooled the north side throughout the simulation; it reached –35 $W \cdot m^{-2}$ at 17:00 LST.

On the south side, the solar flux peaks at noon as expected. Convection and conduction mirror it closely, moving the heat gained from the sun to the air and into the tree interior. In the evening, conduction warms the southernmost point as it cools below the temperature of the tree interior and the tree surface just to the west.

Sensitivity tests

We tested the sensitivity of the model to changes in six variables. Three of these, wind speed (u), wind direction (θ), and solar flux (S), are atmospheric properties. Two others, conductivity (k) and heat capacity (ρc), are thermal properties of the wood. The sixth parameter is moisture content (M), and while it is not explicitly used by the model, it influences ρc and k as discussed in the previous section and so may affect simulation results.

For the sensitivity tests, we used the live aspen case presented in the previous section as a baseline. Each test parameter was then increased or decreased by 5 to 50% of its base value, depending on the parameter. The impact of the change on noon temperatures was noted for the south and north aspects.

Because the test parameters vary widely in magnitude (from k on the order of 10^{-1} to ρc on the order of 10^7) we chose to express model sensitivity, λ, as the ratio of fractional temperature (T) change to fractional parameter (X) change:

$$[12] \quad \lambda = \frac{T_{test} - T_{base}}{T_{base}} \left(\frac{X_{test} - X_{base}}{X_{base}} \right)^{-1}$$

Fig. 2. Observed (diamonds) and modeled (triangles) temperatures for pine-log simulations for (*a*) north, (*b*) east, (*c*) south, and (*d*) west aspects. The broken line with "×" symbols in Fig. 2*a* shows observed air temperatures.

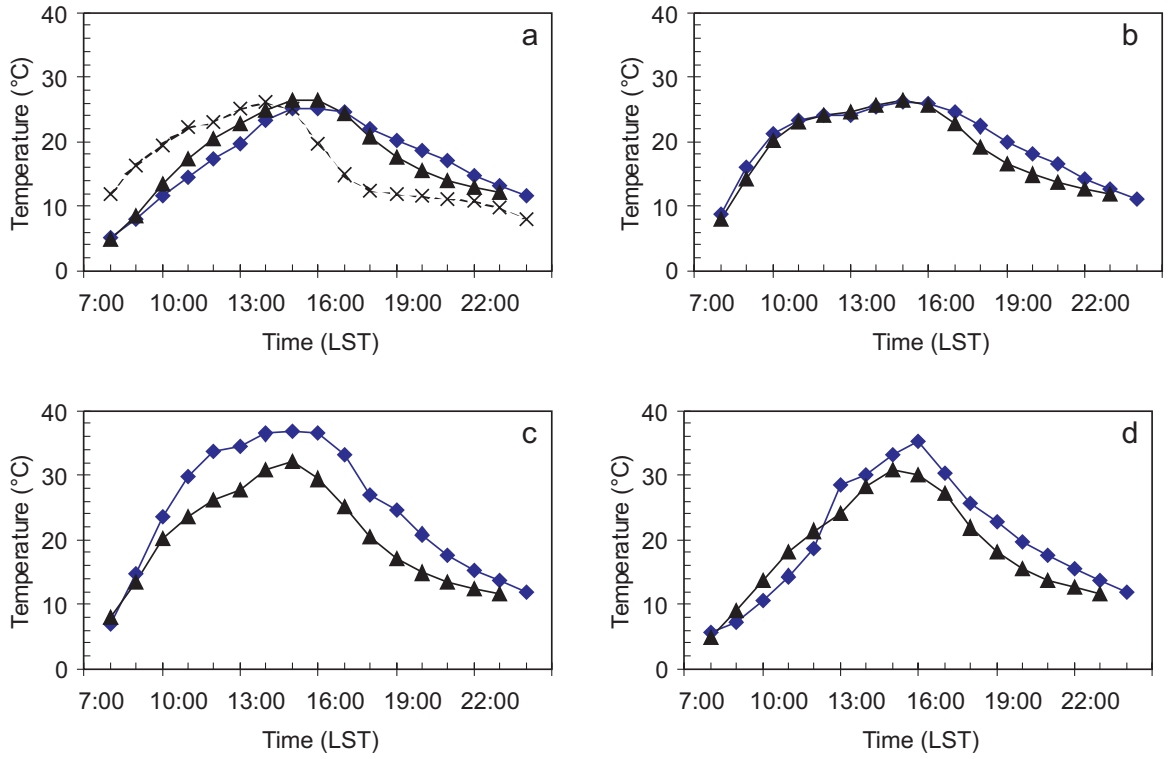

Table 2. Model mean temperature error and root mean square temperature error (RMSE).

	Pine-log simulations		Live-aspen simulations	
Aspect	Mean error (°C)	RMSE (°C)	Mean error (°C)	RMSE (°C)
North	0.2	2.1	2.3	3.0
East	–1.3	1.8	1.4	2.3
South	–5.0	5.6	4.0	4.4
West	–1.7	3.4	3.7	4.3
Overall	–1.9	3.5	2.9	3.6

where λ has a subscript of "s" or "n" to indicate sensitivity on either the south or north aspect.

Table 3 summarizes the results of the tests. Solar flux is clearly the most sensitive of these parameters, while wind speed is the least sensitive. Three parameters, *u*, *k*, and *M*, have opposing sensitivities on the south and north faces. Four parameters, *u*, θ, *S*, and *M*, have a greater impact on the south-aspect temperatures than on the north-aspect temperatures. We discuss reasons for and implications of this in the next section.

Sensitivity tests on θ showed significant nonlinearity. Shifting the wind in the tests from westerly to slightly southwesterly had a strong effect ($\lambda_s = 0.54$) on south-aspect temperatures and very little effect on the north-aspect temperatures ($\lambda_n = 0.02$). When we shifted the wind to be slightly northwesterly, there was a smaller effect ($\lambda_s = 0.06$) on the south aspect and a larger magnitude, negative effect on the north aspect ($\lambda_n = -0.13$).

Discussion

These tests show that the model can reproduce the qualitative features of tree temperatures. Specifically, the observed relationships between various aspects and the timing of their respective temperature peaks are well simulated. The model also succeeds in reproducing the relative amplitudes of daily temperature at the four aspects, and the individual energy fluxes within the model are all of reasonable magnitude. It appears that a model such as the one described here can assist those who hope to understand temperature conditions in and on trees. The model is relatively simple, though computationally intensive, and can be modified to suit specific research questions.

The model errors in the two case studies do not show any strong similarities to one another. Each study had a different aspect where temperatures were most or least accurate. The timing of the greatest errors for any given aspect was also different for each case. The pine simulation results suggest that diffuse solar radiation was an important factor, especially for the north and west aspects. The fact that the east, south, and west aspect temperature peaks were all too low, while the north aspect was too warm, suggests that eq. 11 underestimated direct insolation, and that diffuse radiation was well estimated. Albedo or convection errors would not yield this pattern, but excess conduction from south and west to the north aspect is another possible explanation for the model temperature patterns. The aspen simulation appears to have been too warm, overall. This could easily be because we used full analytical insolation for this simulation. Diffuse solar flux is the cause of the excessive warmth on the north and west faces, as one can infer from Fig. 4.

Fig. 3. Observed (diamonds) and modeled (triangles) temperatures for live-aspen simulations for (*a*) north, (*b*) east, (*c*) south, and (*d*) west aspects. The broken line with "×" symbols in Fig. 3*a* shows observed air temperatures.

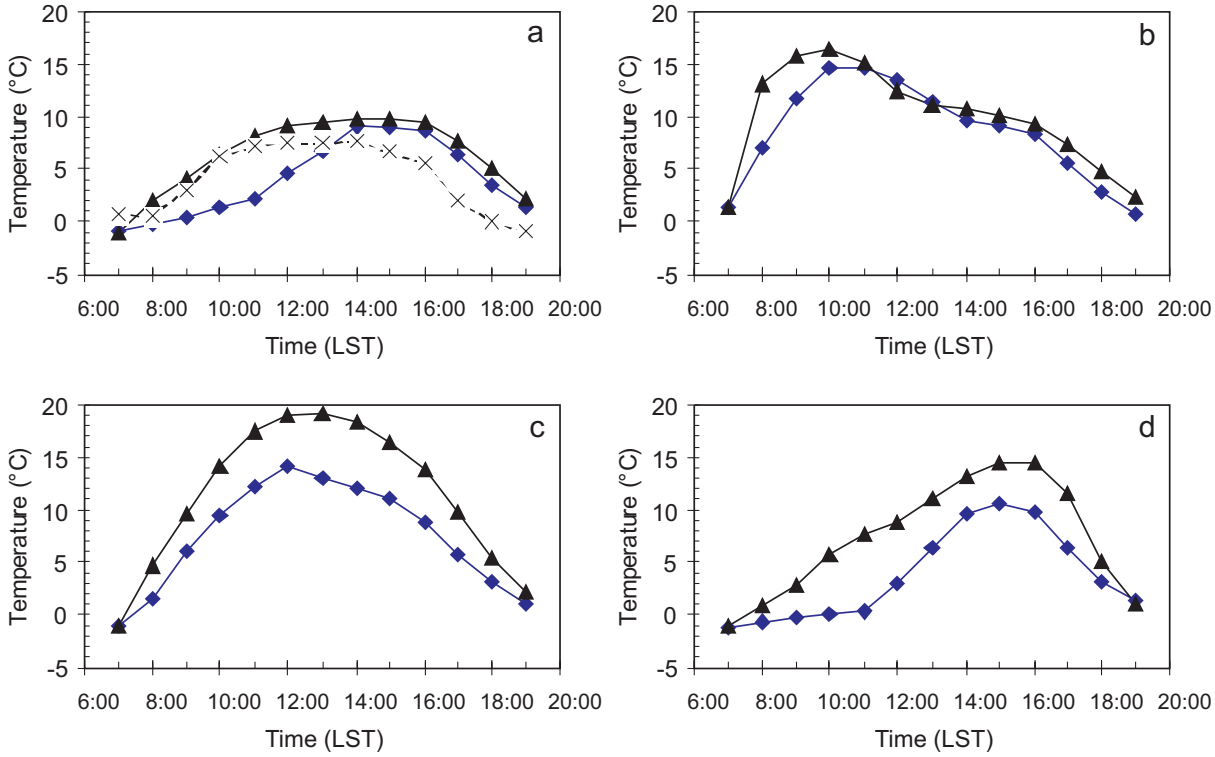

Interpreting the sensitivity results qualitatively is straightforward. Increased u brought north and south aspects closer to ambient air temperature, yielding λ_s and λ_n with opposite signs. Increased θ (a clockwise shift of winds from west to northwest) meant less wind on the south, so south aspect temperature increased and λ_s was positive. Since air temperature was greater than north-aspect temperature, λ_n was also positive. Increasing S affected both diffuse and direct solar radiation, leading to increased temperature everywhere, but larger increases on the south side. Increasing k led to faster equalization of north- and south-aspect temperatures, cooling the south and warming the north; λ_s and λ_n having opposite signs. Increasing ρc reduced the rate of temperature change everywhere, and since the simulations covered a warming period, the result was negative values of λ_s and λ_n.

The influence of M is nonlinear and can vary. Increasing M will always increase ρc and k. Since increasing each of these terms reduced south-aspect temperature, increasing M does the same. However, increased k raised north-aspect temperature while increased ρc slows the rate of all heating or cooling processes, leading to lower north-aspect temperatures. Which of these two effects is stronger varies from case to case, but here the equalizing effects of k dominated.

We feel it important to emphasize the limitations of the sensitivity tests. Because of the interaction of the many model parameters, our tests only give a general idea of how sensitive the model can be. The model proved relatively insensitive to wind speed here, but if the wind had been directed against the south face, where solar heating causes a large air–tree temperature difference, then small changes in wind speed may have caused larger changes in south-aspect temperature. Similarly, had the tests examined afternoon or evening temperatures, the results would have differed.

Table 3. Model sensitivity (λ) to several key parameters.

Parameter	λ_s*	λ_n*
u	–0.01	0.00
S	0.62	0.28
k	–0.15	0.10
ρc	–0.09	–0.18
M	–0.24	–0.05
θ	0.30	–0.06

Note: u, wind speed; S, solar flux; k, conductivity; ρc, heat capacity; M, moisture content; θ, wind direction.

*Subscripts "s" and "n" refer to the south and north aspect of the tree, respectively.

Moisture and bark properties are two areas where the model is weak. Moisture content is not uniform within a tree, and this affects the conductivity, density, and specific heat of the wood. If small, internal temperature differences are important for a specific application, these parameters must be measured. The model is fully capable of using spatially variable moisture and thermal properties, but the actual distribution of these must be known first.

With respect to a tree's surface, evaporation or condensation on the bark will affect the energy balance at the tree's surface (and subsequently within the tree). This can be especially critical for high-temperature simulations such as those involving fire. In these cases, the energy required to evaporate moisture contained within the bark becomes important,

Fig. 4. Modeled energy fluxes for (*a*) north- and (*b*) south-aspect surface points. Fluxes shown include insolation (▲), net infrared (◆), convection (×), and conduction (●).

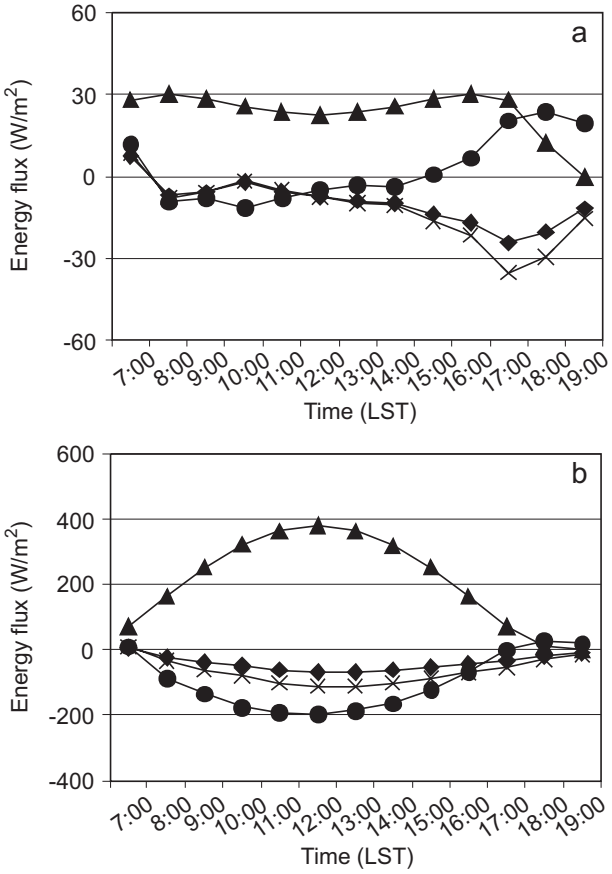

as well. The latter information is not readily available in the scientific literature and would likely depend on the species, age, temperature, and total moisture content of the bark.

A final important aspect of moisture that the model omits is sap flow and the energy it transports along the tree stem. On the north side of a tree, under cloudy conditions, within a tree in an open field, or in winter, the heat carried by sap may be small compared with the other fluxes that the model does represent. But any feature that leads to temperature gradients along the length of the trunk will increase the potential importance of sap heat transport.

Finally, the effects of bark texture on air flow would influence convective heat transfer. This point was raised by Derby and Gates (1966), with a call for research on the topic. It appears that the topic remains unexplored and a worthwhile area for research to address.

Conclusions

We examined the ability of a finite-difference numerical model to simulate heat flow and temperature patterns within a tree stem. The results suggest that such a model can at the least reproduce observed spatial and temporal patterns in the stem. Because we did not have an ideal data set including tree moisture content, thermal conductivity, wood density, observed solar radiation, wind speed and direction, and air and wood temperatures, we could not reasonably test the absolute accuracy of the model. Obtaining such a data set and performing these tests is a priority for future research on the utility of the model.

The parameterizations for convection and solar radiation used here are not appropriate for all situations. Strong winds, large trees, and extreme temperatures all require careful selection or modification of the convective parameterizations. Similarly, cloudy conditions, high elevations, canopy architecture, and smoky situations each present special situations for the parameterization of solar radiation. In some cases the necessary parameterization might already exist, while others would require data collection and creation of an appropriate model.

In spite of the lack of absolute tests of the model, its ability to reproduce the timing of temperature peaks for various aspects and the relative magnitude of the peaks on these aspects is promising. In its present state, the model can be used to examine temperature sensitivity to wind, insolation, moisture, etc. With refinement and appropriate input data, it could be used for specific case studies.

Acknowledgements

The authors wish to thank Stan Wullschleger of Oak Ridge National Laboratory for his review comments and suggested revisions in preparing the manuscript.

References

Andresen, J.A., McCullough, D.G., Potter, B.E., Koller, C.N., Bauer, L.S., Lusch, D.P., and Ramm, C.W. 2001. Effects of winter temperatures on gypsy moth egg masses in the Great Lakes region of the United States. Agric. For. Meteorol. **110**: 85–100.

Derby, R.W., and Gates, D.M. 1966. The temperature of tree trunks—calculated and observed. Am. J. Bot. **53**: 580–587.

Dickenson, S., and Wheeler, B.E.J. 1981. Effects of temperature, and water stress in sycamore, on growth of *Cryptostroma corticale*. Trans. Br. Mycol. Soc. **76**: 181–185.

Eggert, R. 1944. Cambium temperatures of peach and apple trees in winter. Proc. Am. Soc. Hortic. Sci. **45**: 33–36.

Forest Products Laboratory. 1987. Wood handbook: wood as an engineering material. U.S. Dep. Agric. Agric. Handb. 72.

Gill, A.M., and Ashton, D.H. 1968. The role of bark type in relative tolerance to fire of three central Victorian eucalypts. Aust. J. Bot. **16**: 491–498.

Greaves, T. 1965. The buffering effect of trees against fluctuating air temperature. Aust. For. **29**: 175–180.

Haltiner, G.J., and Williams, R.T. 1980. Numerical prediction and dynamic meteorology, 2nd ed. John Wiley & Sons, New York.

Hare, R.C. 1965. Contribution of bark to fire resistance of southern trees. J. For. **63**: 248–251.

Hayes, A.J., and Manap Ahmad, A. 1975. The infection of Corsican pine by *Crumenula sororia* Karst. Forestry, **48**: 183–191.

Hengst, G.E., and Dawson, J.O. 1994. Bark properties and fire resistance of selected tree species from the central hardwood region of North America. Can. J. For. Res. **24**: 688–696.

Herrington, L.P. 1969. On temperature and heat flow in tree stems. Yale Univ. Sch. For. Bull. 73.

Kreith, F., and Bohn, M.S. 1986. Principles of heat transfer. 4th ed. Harper & Row, New York.

Lowry, W.P., and Lowry, P.P., II. 1989. Fundamentals of biometeorology: interactions of organisms and the atmosphere.

Vol. I: The physical environment. Peavine Publications, McMinnville, Oreg.
Shepherd, R.F. 1966. Factors influencing the orientation and rates of activity of *Dendroctonus ponderosae* Hopkins (Coleoptera: Scolytidae). Can. Entomol. **98**: 597–518.
TenWolde, A., McNatt, J.D., and Krahn, L. 1988. Thermal properties of wood and wood panel products for use in buildings. U.S. Dep. Energy Rep. DOE/USDA-21697/1.
Vines, R.G. 1968. Heat transfer through bark, and the resistance of trees to fire. Aust. J. Bot. **16**: 499–514.
Weast, R.C. 1980. CRC handbook of chemistry and physics. 60th ed. CRC Press, Boca Raton, Fla.

Appendix A

The convective heat transfer coefficients presented for free convection in eq. 4 are from Kreith and Bohn (1986). The provided parameterized coefficient is in non-SI units, and eq. 4 involved some manipulation as well as simple unit conversion; this Appendix derives the formula in SI units.

Kreith and Bohn (1986) states that the heat transfer coefficient, h, for free convection is

$$[A1] \quad h = \mathrm{Nu}\frac{k}{L}$$

where Nu is the nondimensional Nusselt number, k is a function of temperature in $W \cdot m^{-3} \cdot K^{-1}$, and L is the length of the surface element under consideration.

Following Kreith and Bohn and converting to SI units:

$$[A2] \quad k = 2.11 \times 10^{-4}(T_{air} + 97.77)$$

with T_{air} in Kelvins. The Nusselt number, Nu, is

$$[A3] \quad \mathrm{Nu} = 0.555(\mathrm{Pr} \times \mathrm{Gr})^{0.25}$$

where Pr is the Prandtl number (0.71 for air, Weast 1980) and Gr is the Grashof number, both nondimensional. The Grashof number is

$$[A4] \quad \mathrm{Gr} = \frac{L^3 \rho g \beta \Delta T}{\mu^2}$$

with ρ the density of air, g the acceleration resulting from gravity, β the coefficient of bulk expansion for air, ΔT the temperature difference between the surface and the air, and μ the viscosity of air. Using data from Weast (1980) for viscosity between temperatures of 18°C and 500°C, we computed a regression of μ as a function of T_{air}:

$$[A5] \quad \mu = (69.64 + 0.389T_{air}) \times 10^{-7}$$

where T_{air} is in Kelvins and μ is in $kg \cdot m^{-1} \cdot s^{-1}$. From this and the ideal gas law, eq. A4 becomes

$$[A6] \quad \mathrm{Gr} = L^3 \Delta T \frac{1.22 \times 10^{20}}{T_{air}^3 (69.64 + 0.39T_{air})^2}$$

Combining eqs. A1, A2, A3, and A6 and simplifying yields eq. 4.